A PERMEABILITY APPARATUS AND SEEPAGE INDUCED DEGRADATION OF SOFT ROCK

Yii-Wen Pan[1] and Heng-You Chen[2]

ABSTRACT

The conventional methods of laboratory permeability test may not be appropriate for soft rock. In this paper, an apparatus was developed for determining rock permeability using flow-pump approach and allowing for the control over the specimen confining pressure and saturation. Results from the flow-pump permeability tests verify the capability of this apparatus which is specially designed for soft rocks. The presented work shows that the permeability of soft rock considerably depends on the subjected confining pressure and loading history. The permeability anisotropy of a soft rock was also explored by testing specimens prepared along different orientations.

Besides the permeability tests, the effect of seepage on the microstructure of poorly cemented sandstone were investigated by examining the microscopic features of the tested rock material using sectioned specimens obtained before and after the seepage flow. The objective is to investigate the possible degradation due to seepage. By comparing the microstructure before and after seepage, it was found that the porosity of the rock material increases and results in degradation. Its reason is probably due to that fines particles or infill materials were moved away as a result of internal erosion along with seepage flow. On the other hand, other major texture parameters (including grain area, equivalent diameter, major axis angle, elongation, and roundness) are not affected by seepage.

Key words: Soft rock, permeability apparatus, degradation, seepage, microstructure, texture.

1. INTRODUCTION

Soft rocks belong to a category of weak rocks (ISRM, 1981; Johnston, 1993; Oliveira, 1993) and may be regarded as a transitional geo-material (*i.e.*, between soils and hard rocks). This type of geo-material usually presents characteristics including poor cementation, low strength and high deformability (Johnston, 1995). The poorly cemented sandstone, often appear along the northern and western foothill in Taiwan, is one example of soft rocks. In young soft rock, the presence of fractures or joints is usually not very significant.

Rainfall infiltration or water head difference results in seepage flow through a rock stratum. Permeability is a required parameter for a seepage analysis. For soft rock without significant fractures, the permeability of intact rock in laboratory may be quite close to the in-situ permeability. In general, laboratory permeability tests can be conducted by forcing a longitudinal flow or a radial flow in the rock specimen (Lama and Vutukuri, 1978). However, these conventional methods of permeability test may not be appropriate for soft rock.

For a permeability tests in radial flow, a donut-like hollow cylinder specimen has to be prepared. A radial flow is enforced by applying a head difference between the inside and outside boundaries of the specimen. For a poorly cemented soft rock, the preparation of a hollow cylinder specimen for radial flow test may be very difficult because of possible specimen breakage during inevitable over-coring process.

Longitudinal flow permeability test makes use of a cylindrical specimen; hence, specimen preparation is much easier in this case. The test employs a condition of constant or falling head difference between two ends of the tested specimen. The permeability test has to collect the amount of water flowing out of the specimen over a period of time. For a tested material with very low permeability, this task would require a long time to improve accuracy.

No matter which testing method is employed, the permeability of a geo-material is highly dependent of the degree of specimen saturation. The quantitative control of specimen saturation in a permeability test is not very easy in the conventional methods (Lama and Vutukuri, 1978). Olson *et al*. (1988) proposed the flow-pump method for testing soil permeability in a triaxial cell. A permeability test using flow pump, instead of controlling the head difference, forces a constant amount of flow rate into a specimen (ASTM, 1993; Olson *et al*., 1988). In the test, the head difference between two ends of the specimen is measured. With the employed flow rate and the measured head difference, one thus can calculate the permeability of the tested specimen.

Combining the flow-pump and a triaxial cell, both confining pressure and back pressure can be applied to the specimen. The advantages of this combination are three fold. First, the applied back-pressure can raise the degree of saturation of the tested specimen. Second, the permeability of a specimen under various confining pressure can be determined without difficulty. Third, a triaxial compression test, if necessary, can be carried out using the same specimen immediately after the permeability test, with no need of specimen re-installation and re-saturation for the triaxial compression test.

Soft rock tends to degrade when it is exposed to unfavorable environmental conditions (Ocepek and Logar, 2008). The degra-

Manuscript received February 25, 2009; revised August 16, 2009; accepted August 17, 2009.

[1] Professor (corresponding author), Department of Civil Engineering, National Chiao Tung University, Hsinchu 30050, Taiwan, R.O.C. (e-mail: ywpan@mail.nctu.edu.tw).

[2] Former Graduate Student, Department of Civil Engineering, National Chiao Tung University, Hsinchu 30050, Taiwan, R.O.C.

dation of soft rock often results in the reduction of its strength and deformability (Tatsuoka, 1995; Tatsuoka *et al*., 2003). Among other possible causes of degradation, a continuous seepage flow through poorly cemented rock may induce leaching or internal erosion (the transport of fine materials is referred to as "internal erosion") of fines or infill material in the geo-material (Nikraz, 1998). Internal erosion may cause porosity increase and material degradation, and can be regarded as one kind of weathering process. It is of interest to understand the possible cause of seepage induced degradation by means of observation for the microstructure change of weak sandstone after seepage.

The objectives of this paper are as follows. First, an apparatus, specially designed for soft rock, was developed for determining the permeability of soft rock using the flow-pump approach. This apparatus allows the controls over specimen confining pressure as well as its saturation. The design concepts and testing procedures for this apparatus are described. Experimental results from the permeability test are presented with discussion. Subsequently, we compared the microstructure of poorly cemented sandstone before and after the application of seepage flow using sectioned rock specimens. Its aim is to investigate the microstructure difference of poorly cemented sandstone before and after seepage induced degradation.

2. FLOW-PUMP APPARATUS FOR ROCK PERMEABILITY

2.1 Description of the Apparatus

The developed apparatus adopted the flow-pump approach (Olson *et al*., 1988) for measuring rock permeability. This apparatus, as Fig. 1 shows, is capable of carrying out constant flow permeability tests. This system contains four parts, namely: (1) a flow pump, (2) a multi-purpose triaxial cell, (3) data measurement and acquisition, and (4) pressure supply and controls. In Fig. 1, "W" denotes water, "S" denotes the tested specimen, and "DPT" denotes the differential pressure transducer. Further explanations are as follows.

Figure 2 shows the picture of the flow pump. The flow pump contains a servomotor and an actuator. The servomotor, connected to the actuator, is capable of controlling linear motion of piston at various speeds (within 1.67×10^{-8} and 3.33×10^{-5} m/s). Figure 3 presents the design concept of the actuator. The actuator is made of a solid piston in a metal flow tube; this piston is designed such that the cross section areas at its two ends (in and out) differ only slightly. The space between the flow tube and the piston is filled with water through the top drainage. Water can flow in and out the flow tube through the bottom drainage path which is connected to the tested specimen. As the piston move forward, the volume between the tube wall and piston reduces, thus water is squeezed out; and vice versa. By controlling the speed of servomotor, the flow rate can be controlled accordingly. Since the flow rate can be calibrated against the controllable piston speed, the control of a very small constant flow rate can be achieved using the actuator with the piston inside. The flow rate can be controlled in the range of $4.3 \times 10^{-9} \sim 2.1 \times 10^{-12}$ m^3/s.

The multi-purpose triaxial cell was specifically designed for testing the mechanical properties of soft rock (Huang *et al*., 2001). The wall of the triaxial cell was made of stainless steel

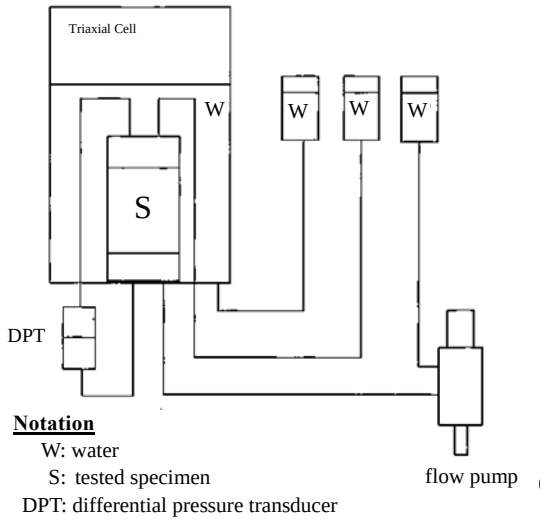

Fig. 1 Layout of the permeability test system

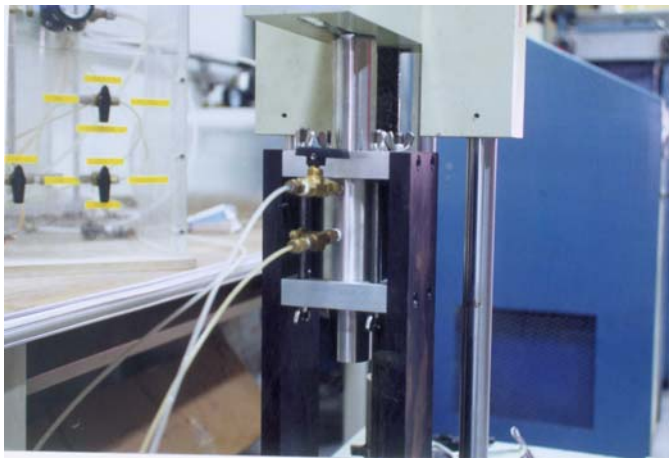

Fig. 2 Flow pump

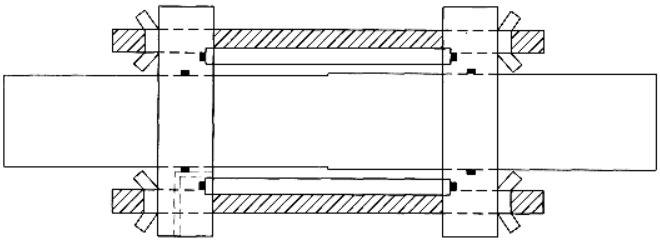

Fig. 3 Actuator of flow pump

capable of sustaining a maximum cell pressure of 15 MPa. Four vertical inner struts were designed to enhance easy assemblage of the whole cell. Both the bottom and top plates of the triaxial specimen can be connected to drainage paths. The drainage paths allow the passage of water, application of back-pressure, or measurement of pore water pressure. The design of the triaxial cell also includes several feed-through connectors allowing for in-vessel measurements such as local strain measurement and internal load cell inside the triaxial cell. When necessary, servo-controlled tests can be carried out using the multi-purpose triaxial cell (Fig. 4). Detail description of the triaxial system is beyond the scope of the presented paper.

Fig. 4 Multi-purpose triaxial cell

The cell pressure and the back-pressure are measured by pressure transducers for pressure up to 1.4 MPa. A differential pressure transducer (range: ±24 kPa) measures the pressure difference between two ends of a cylindrical specimen. An analog/digital conversion card (Advantec PCL-816) installed in a personal computer allows the transformation of the data from analog signals into digital data and stores the digital data on a computer disk.

An air compressor with a capacity of 1 MPa supplies the air pressure that provides the pressure source of confining pressure and back-pressure. The applied confining pressure and the back-pressure are controlled by double regulators to raise the accuracy and stability of the applied pressures.

2.2 Procedure of Constant Flow Permeability Test

The constant flow permeability test follows the following procedure.

1. Prepare the cylindrical specimen. Cylindrical specimens were drilled from a block sample in laboratory. During drilling, foam instead of water was used as the drilling fluid in order to avoid the drilling water weakening the soft rock during the drilling process. Determine the weight *W*, the diameter, *D*, and the length, *L*, of the specimen. The specimens were NX-sized, and the (*L*/*D*) ratio of cylindrical specimen was about 2.2.
2. Place filter papers on both the top and bottom faces of the specimen, then place the top and bottom porous plates. Cover the specimen by a rubber membrane, then fix two ends to porous plates by rubber bands.
3. Connect all necessary tubing and transducers. Fill the triaxial cell with de-aired water and apply the cell (confining) pressure. Apply pressure at one end of the specimen; allow water flowing through specimen to remove pore air.
4. Close drainage valves; apply back-pressure. Carry out $\overline{B}$-check as follows. Increase confining pressure and measure the change in pore water pressure in order to check the Skempton's pore pressure coefficient $\overline{B}$ (= pore pressure change divided by the confining pressure change). Increase the back-pressure and confining pressure level. The $\overline{B}$ value increases with the degree of saturation (S_r). S_r can be raised by back pressure; thus, $\overline{B}$ increase with the back pressure. The $\overline{B}$ value will gradually become stable as S_r approaches 100%. Repeat the $\overline{B}$ check until $\overline{B}$ reaches a stable value. When the specimen is not yet saturated, the $\overline{B}$ value tends to increase with the applied back-pressure, or the air trapped in the pores tends to result in an oscillation of pressure difference between two ends of specimen, which can be observed from the differential pressure transducer. Usually, the back pressure required for a stable value of $\overline{B}$ for the tested specimens was about 0.2 MPa.
5. Turn on the servomotor after the water pressure at the two ends of the sample equilibrates; allow a flow rate of *q* flowing through the specimen. Measure the head difference Δh across the specimen after it becomes stable. If necessary, the direction of the servomotor can be reversed to force water to flow in the reverse direction; then, re-measure the head difference after it becomes stable.

2.3 Calculation of Permeability

Figure 5 shows a typical plot of head difference versus time for a constant flow permeability test using the developed apparatus. In the test, the cell pressure and the back pressure are 0.3 MPa and 0.21 MPa, respectively. The controlled flow rate is 1.29×10^{-9} m^3/s. As the seepage flows upward, the head difference is 98.6 mm. As the seepage flows downward, the head difference is 98.5 mm. The average head difference is 98.55 mm. For each phase of seepage flow (upward flow and downward flow), the duration is about 30 minutes.

The permeability hence can be calculated by the Darcy's Law:

$$k = \frac{qL}{A\Delta h} \tag{1}$$

in which *k* is the coefficient of permeability of the specimen, *q* is the flow rate, *L* is the specimen length, *A* is the cross sectional area, and Δh is the measured head difference between two ends of the specimen.

For the demonstrated case, the coefficient of permeability can be calculated as 6.95×10^{-5} cm/s (1 cm/s = 10^{-2} m/s). With a series of different controlled flow rate for a same specimen, one can obtain the relation between flow rate and hydraulic gradient. Figure 6 shows the relations between the induced hydraulic gradient and the flow rate; a linear relationship is notable. It confirms the validity of Darcy's Law over the range of the tested flow rate.

3. EXPERIMENTS RESULTS

3.1 Samples

A series of permeability experiments were carried out on some soft sandstones sampled from the west foothill region of Taiwan. Samples from the Pliocene Cholan Formation near Da-Ken, Taichung and from the Pliocene-Pleistocene Toukoshan Formation near Bao-Shan, Hsinchu were used in this study. These sandstone formations were in general poorly cemented and

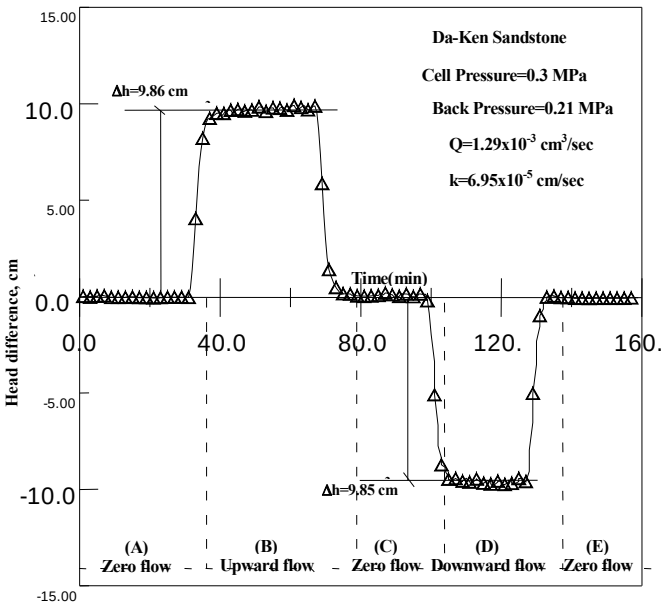

Fig. 5 Typical plot of head difference versus time in permeability test

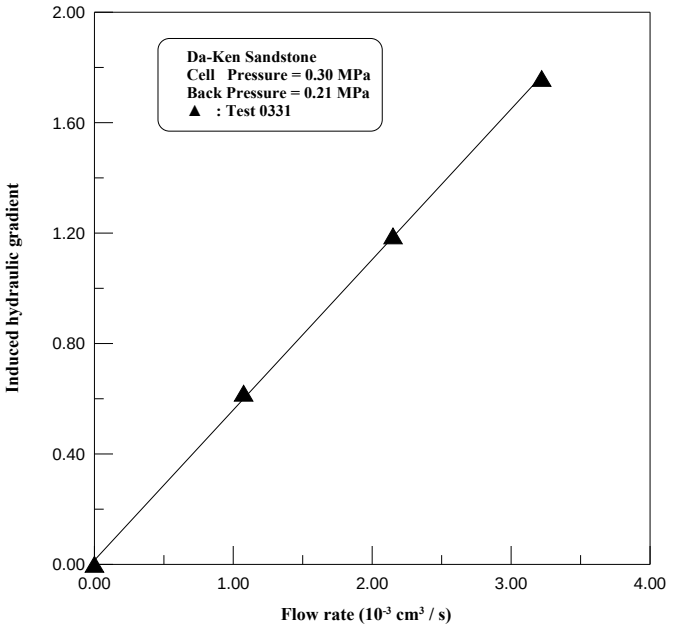

Fig. 6 Plot of induced hydraulic gradient versus flow rate

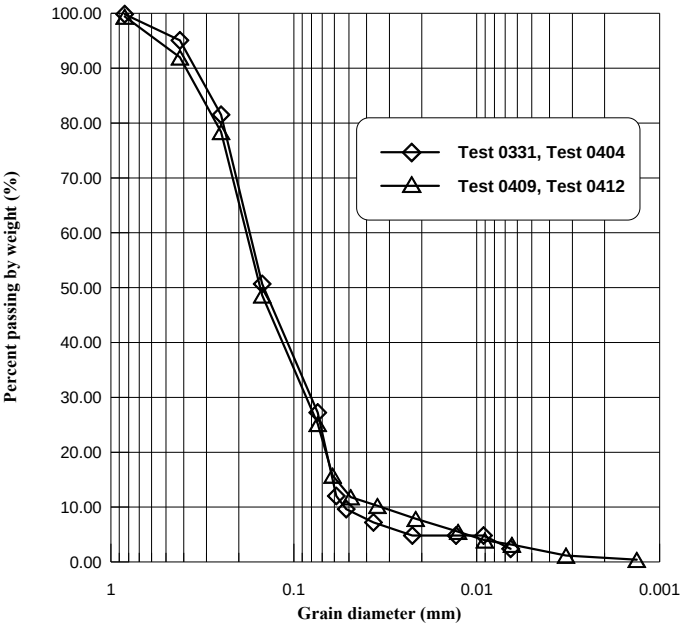

Fig. 7 Typical grain size distribution of Da-Ken yellowish sandstone

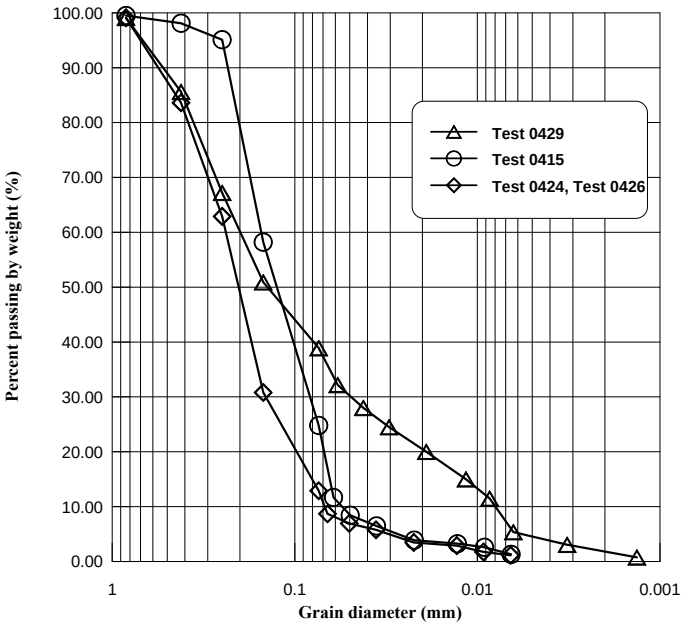

Fig. 8 Typical grain size distribution of Bao-Shan yellowish sandstone

easily degradable when exposed to water. The uni-axial strength of the sandstone samples from Da-Ken was in the range of 7 ~ 13 MPa. The uni-axial strength of the sandstone samples from Bao-Shan was in the range of 0.5 ~ 4 MPa. Figures 7 and 8, respectively, show the typical grain size distributions of the two poorly cemented sandstones sampled from Da-Ken and Bao-Shan, respectively.

3.2 Range of Permeability and Consistency of Results

The overburden depth at the sampled site of the block samples was within 10 ~ 15 m. Therefore, a series of permeability tests were carried out under the effective confining pressure 0.2 ~ 0.3 MPa (to match the in-situ stress level) to examine the consistency of the test results. For each specimen, a series of different controlled flow rates were employed, the head differences were measured, and the corresponding values of permeability were calculated. Table 1 presents the results of a series of tests.

The values of permeability of Da-Ken yellowish sandstone were in the range of $3 \times 10^{-5} \sim 9 \times 10^{-5}$ cm/s. The stratum in Bao-Shan sandstone was composed of alternate yellowish sandstone and gray silty sandstone. The values of permeability were about 3×10^{-4} cm/s for Bao-Shan yellowish sandstone, and about 9×10^{-6} cm/s for Bao-Shan gray silty sandstone. A series of Lugeon tests were also carried out at the site where the block samples of Bao-Shan sandstone were taken. In the similar stratum and with

Table 1 Results of permeability tests

Sample source	Rock type	Test No	Confining pressure (MPa)	Back pressure (MPa)	Flow rate (cm^3/s)	Head difference (cm)	Hydraulic gradient	Coefficient of permeability (cm/s)
Da-Ken, Taichung	Yellowish sandstone	Test 0331	0.3	0.21	3.22×10^{-3}	20.00	1.76	7.9×10^{-5}
					2.15×10^{-3}	13.50	1.19	8.3×10^{-5}
					1.08×10^{-3}	7.00	0.62	8.0×10^{-5}
	Yellowish sandstone	Test 0404	0.3	0.21	1.29×10^{-3}	9.85	0.86	7.0×10^{-5}
					0.86×10^{-3}	5.90	0.52	7.7×10^{-5}
					0.43×10^{-3}	2.80	0.24	8.2×10^{-5}
	Yellowish sandstone	Test 0409	0.3	0.21	1.72×10^{-4}	3.12	0.27	2.9×10^{-5}
					3.44×10^{-4}	5.78	0.49	3.2×10^{-5}
					5.16×10^{-4}	9.20	0.78	3.0×10^{-5}
Bao-Shan, Hsinchu	Yellowish sandstone	Test 0415	0.2	0.16	1.08×10^{-3}	1.80	0.15	3.1×10^{-4}
					2.15×10^{-3}	3.57	0.30	3.1×10^{-4}
					3.22×10^{-3}	5.30	0.45	3.2×10^{-4}
	Yellowish sandstone	Test 0424	0.2	0.12	4.30×10^{-4}	0.85	0.07	2.7×10^{-4}
					8.60×10^{-4}	1.66	0.14	2.7×10^{-4}
					12.90×10^{-4}	2.38	0.20	2.8×10^{-4}
	Gray silty sandstone	Test 0429	0.3	0.21	6.45×10^{-5}	3.82	0.36	8.6×10^{-6}
					1.29×10^{-4}	7.22	0.63	9.1×10^{-6}
					1.94×10^{-4}	11.55	1.01	8.6×10^{-6}

the similar overburden, the Lugeon test obtained the test result of 40.9 Lugeons. Using the rule of thumb of 1 Lugeon for 1.0×10^{-5} cm/s, the estimated permeability from the Lugeon test would be 4.1×10^{-4} cm/s. This estimated value of permeability appears consistent with the permeability of the Bao-Shan yellowish sandstone obtained from the laboratory tests. The good agreement of laboratory and in-situ permeability test was reasonable since there are little fractures or joints found in the formation of the Bao-Shan sandstone.

3.3 Influence of Confining Pressure on Permeability

Wilbur (1990) studied the influence of normal stress on fracture transmissivity. The effective confining pressure may also affect the permeability of intact rock. Permeability tests of a specimen subjected to various effective confining pressures were further carried out to study the influence of confining pressure on the permeability of soft rock. Specimens of Bao-Shan yellowish sandstone were subjected to a series of effective confining pressure during the permeability test. The sequence of the effective confining pressures was applied as follows: 0.08 MPa → 0.18 MPa → 0.28 MPa → 0.38 MPa → 0.28 MPa → 0.08 MPa. One permeability test was carried out for each step in the series. Figure 9 depicts the influence of confining pressure on the permeability. It is clearly shown that permeability decreases while the confining pressure increases. However, the change was within the same order in the range of tested pressures. Also observable in Fig. 9, the permeability is slightly lower while the confining pressure unloads back to the same pressure level.

3.4 Anisotropy in Permeability

The appearance of the soft rock from Da-Ken and Bao-Shan does not show obvious sign of anisotropy in general. Nevertheless, an attempt was made to examine the anisotropy in their permeability. One Da-Ken sandstone specimen was drilled along the direction parallel to the bedding plane (denoted the specimen *P*), while another one was perpendicular to the bedding plane (denoted the specimen *V*). Both specimens were subjected to the same test conditions maintaining a constant seepage flow. The sequence of the effective confining pressures was applied as follows: 0.05 MPa → 0.1 MPa → 0.2 MPa → 0.4 MPa → 0.2 MPa → 0.1 MPa → 0.05 MPa. Figures 10 and 11, respectively, depict the permeability under various confining pressures. It appears that the permeability for the specimen with its axis parallel to the bedding plane is in general 25 ~ 30% larger than the permeability for the specimen with its axis perpendicular to the bedding plane. These results also re-confirm the effects of confining pressure and loading history on the permeability of the tested soft rock.

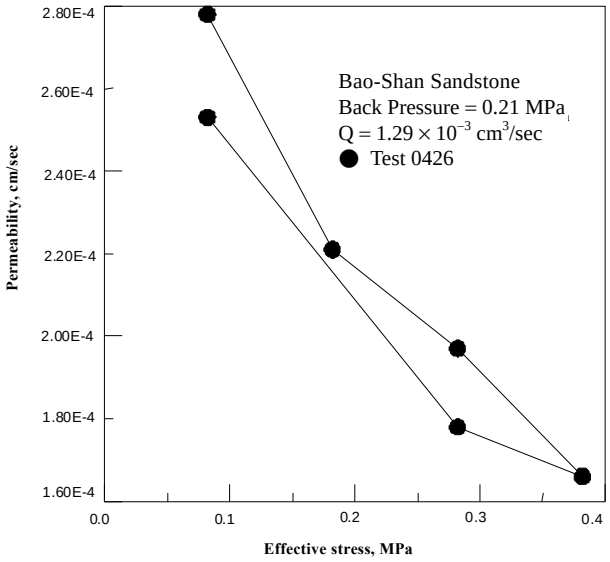

Fig. 9 The influence of confining pressure on permeability

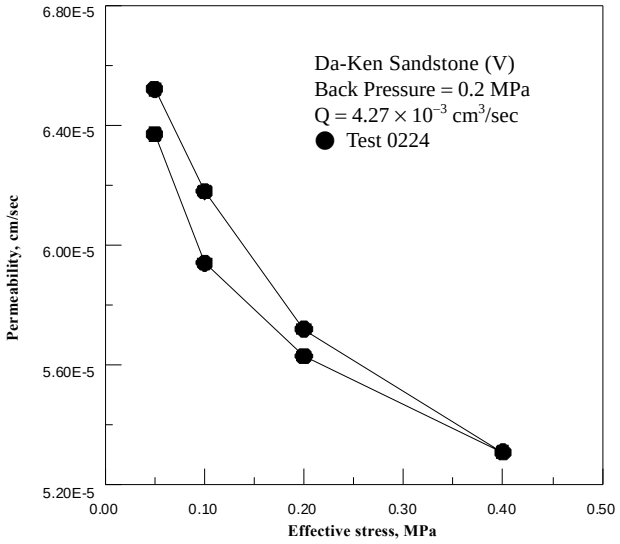

Fig. 10 Permeability versus effective confining pressure for specimen *V*

4. COMPARISON OF MICROSTRUCTURE BEFORE AND AFTER SEEPAGE

4.1 Approach for Microstructure Analysis

Continuous seepage flow through poorly cemented rock may induce leaching or internal erosion of fines or matrix in the geo-material; and may result in material degradation. An attempt was also made to examine the effect of seepage flow on the microstructure of soft rock. Image analysis of the photograph obtained via mineral microscope enables the examination of microstructure (including pores and texture) on the surface of a sectioned specimen. Detection of pore spaces may be enhanced by using fluorescent or colored resins (Nishiyama and Kusuda, 1994). By comparing the microstructure of an identical soft rock samples without and after seepage flow, it is possible to inspect the effect of seepage flow on the microstructure of the soft rock in order to examine the possible seepage induced degradation.

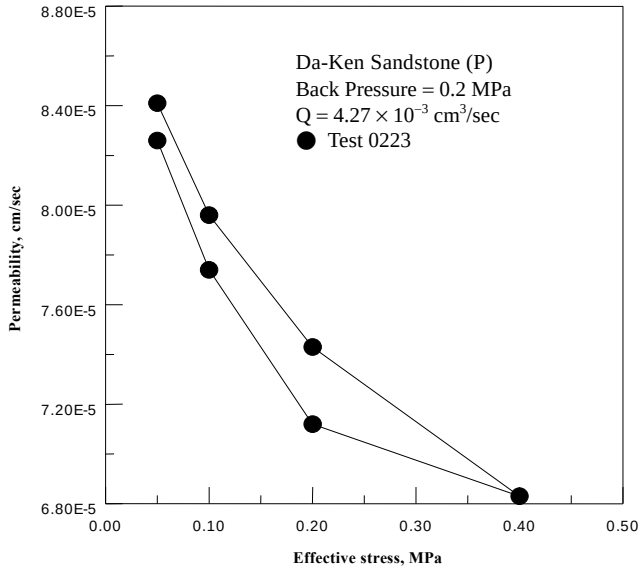

Fig. 11 Permeability versus effective confining pressure for specimen *P*

One original sample without seepage and two remained samples from Test 0331 and Test 0404 after seepage tests were used to prepare sectioned specimens following the procedure illustrated as Fig. 12 shows. The step-by-step procedures, in order, are as follows. (1) Break a specimen into small rock fragments. (2) Submerge a selected rock fragment in pre-mixed glue (which is a mixture containing polyester resin, acetone as a thinner, hardener, and color dye) inside a mold container. (3) Place the mold container inside a vacuum desiccator; then apply vacuum (for 15 minutes) to remove the air trapped in rock fragment. (4) Allow the solidification of the specimen (24 hours). (5) Section the already harden specimen (with glue filling the voids inside the specimen) to make a planar surface; then, polish the planar surface with a polishing apparatus to obtain a final mirror-like surface; the sandy papers on the polishing apparatus were gradually replaced in a sequence of #240, #400, #600, and #1000. To avoid degradation during grinding, ethanol instead of water was used during surface polishing. (6) Fix the polished specimen to a (glass) slide; then place the slide under a microscope to observe the microscopic features of the sectioned rock specimen. The image under the microscope can be captured into a digital image file for further image analysis. The actual size of the image can be calibrated using a micrometer by knowing the enlargement ratio of the eyepiece and the object lens. The size corresponding to the smallest division on the micrometer is 0.01 mm (as shown in Fig. 13).

Two sectioned specimens were prepared for each sample. MS1 and MS2 denote the sectioned specimens prepared from the original sample without seepage. MS3 and MS4 denote the sectioned specimens prepared from the remained samples of Test 0331 which was subjected to a seepage flow rate of 1.29×10^{-9} m^3/s. MS5 and MS6 denote the sectioned specimens prepared from the remained samples of Test 0404 which was subject to a seepage flow rate of 3.22×10^{-9} m^3/s. For each sectioned specimen, five randomly picked image file were extracted for the image analysis and for further statistics in the subsequent discussion of microstructure variables.

Figs. 14, 15, and 16, respectively, are the typical images for MS1, MS3, and MS5, respectively. In these figures, (a) is the raw

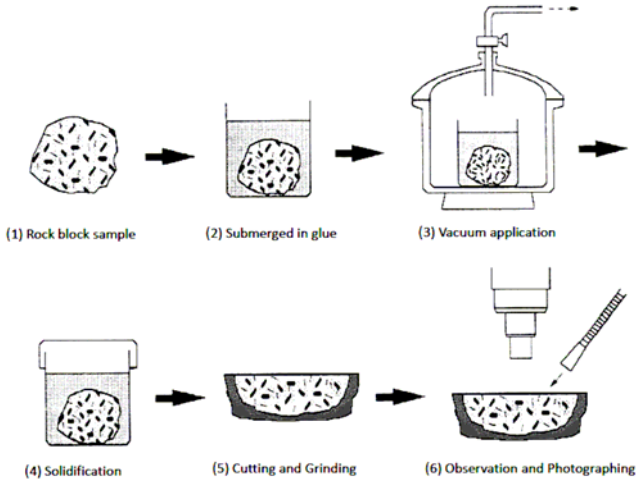

Fig. 12 Illustrated flow chart for making sectioned specimen

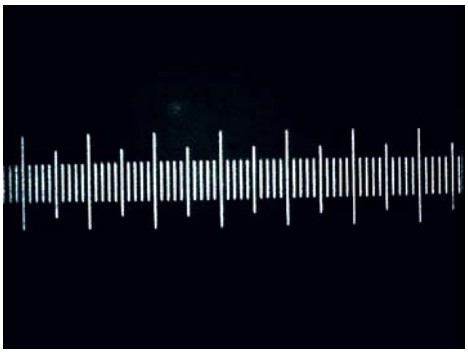

Fig. 13 Image of micrometer for size calibration (enlarged 180 times)

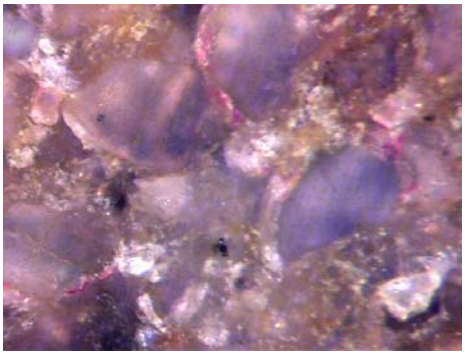

(a) Raw image

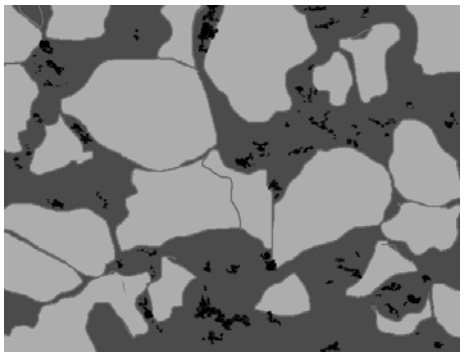

(b) Processed image

Fig. 14 Typical image of sectioned specimen for MS1

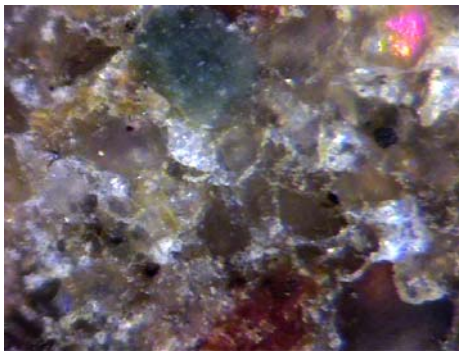

(a) Raw image

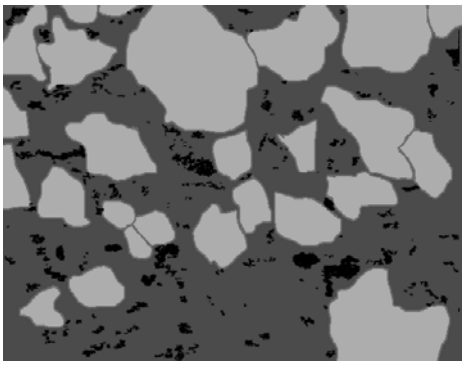

(b) Processed image

Fig. 15 Typical image of sectioned specimen for MS3

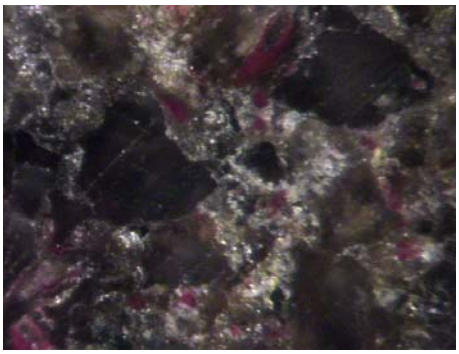

(a) Raw image

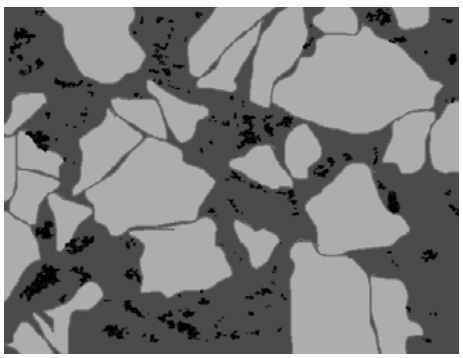

(b) Processed image

Fig. 16 Typical image of sectioned specimen for MS5

picture for the specimen; while (b) is the already processed image showing the partitions of grain, infill (matrix), and void, in sequential order of grey levels. It is easier to identify grains and pore on a raw picture. For scaling reference, the largest grain size shown in these figures are consistently about 0.2 mm. In the image analysis, the boundaries of every grain and pore on each image were located and drawn; the remained portion was taken as infill.

4.2 Porosity before and after Seepage

For a specific image, the number of pixels for each component over the total number of pixels represents the composition ratio of that component in the observed domain. For each sample set, a total of ten images (five images for each of two sectioned specimens) are used for the above-mentioned evaluation and for further statistics.

Figure 17 compares the composition percentages of grain, matrix, and void for each set of specimen. MS1-2 is the set of samples (MS1 and MS2) that were not subjected to seepage. MS3-4 is the set of samples (MS3 and MS4) that were subjected to a seepage flow rate of 1.29×10^{-3} cm^3/s which is corresponding to a hydraulic gradient 0.86. MS5-6 is the set of samples (MS5 and MS6) that were subjected to a seepage flow rate of 3.22×10^{-3} cm^3/s which is corresponding to a hydraulic gradient 1.76. The sample MS1-2 (the one without seepage) has a void percentage 3.15%. The void percentage for samples MS3-4 (which was subjected to hydraulic gradient 0.86) and MS5-6 (which was subjected to hydraulic gradient 1.76), respectively, are 5.26% and 6.23%, respectively.

The increase in porosity is 2% ~ 3% after the application of seepage flow. It appears that seepage flow can cause an increase in the porosity of the tested soft rock. The data also indicates that a higher hydraulic gradient results in a higher porosity increment. This is explainable since a higher hydraulic gradient may imply higher internal erosion intensity in the specimen. Although without sufficient data, it can be inferred that the duration of seepage and total volume of seepage flow may also play a role affecting the internal erosion of soft rock. The duration of seepage flow in each permeability-test set is one hour or so. Accordingly, the total volume of seepage flow through a specimen can be estimated by multiplying the flow rate and duration.

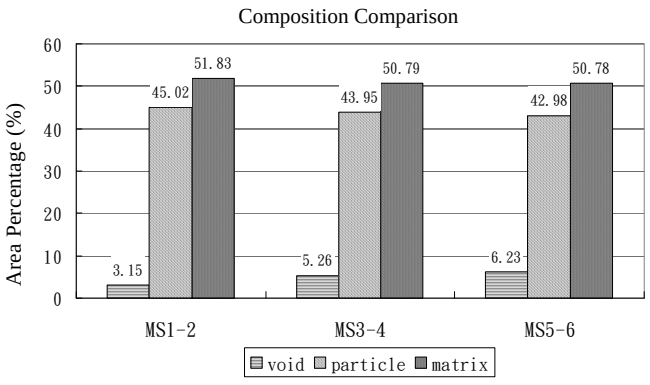

Fig. 17 Comparison of component compositions before and after seepage

The increase of porosity, naturally, is a result of the counterpart reduction in the composition ratio of solid components including grain particles and infill. By a close observation through microscope, it appears that fines particles or resolved infill material were moved away as a result of internal erosion due to seepage. Generally speaking, an increase in porosity is an indication of the degradation of rock material; this may imply reductions in its strength and stiffness, also an increase in its permeability.

4.3 Texture before and after Seepage

The texture of a rock material provides many important information of sedimentary rock. Major parameters concerning texture, among others, may include grain size, shape, arrangement, and so on. The texture parameters may not only reveal the history of sedimentation, but also affect the mechanical behavior and properties of a rock material. The distributions of major texture parameters, before and after seepage, were determined from image analysis to examine whether those parameters are affected by seepage flow.

In the present work, the texture parameters including grain area, Feret diameter, major axis angle, elongation, and roundness were examined. They were determined through image analysis using the free software UTHSCSA Image Tool 3.0 developed and released by the University of Texas Health Science Center. This image tool is for image processing and analysis. The frequency distributions of the texture parameters for the sample sets MS1-2, MS3-4, and MS5-6 were compared and discussed in order.

(1) Frequency Distribution of Grain Area

From image analysis, the area of each grain particle can be obtained. Figure 18(a), (b), and (c), respectively, are the distributions of grain-particle area A obtained from the image sets of MS1-2, MS3-4, and MS5-6, respectively. All of the distributions appear similar; the peak frequency consistently occurs near 0.004 mm^2. More than 75% of grain areas are within 0.002 ~ 0.01 mm^2. The difference of grain-area distribution before and after seepage is not significant.

(2) Frequency Distribution of Ferret Diameter

Ferret diameter D_F is the diameter of a circle that has the same area of an object. It is the equivalent diameter of a particle with an arbitrary shape. Given the object area A, the Ferret diameter thus can be calculated using $D_F = \sqrt{4A/\pi}$. This diameter can be regarded as a measure of equivalent grain size. To plot its frequency distribution, all Ferret diameter are grouped by size in the order of 0.03 mm, 0.05 mm, 0.07 mm, 0.09 mm, 0.11 mm, 0.13 mm, 0.15 mm, 0.17 mm, and > 0.17 mm. Figure 19(a), (b), and (c), respectively, are the distributions of Ferret diameter obtained from the image sets of MS1-2, MS3-4, and MS5-6, respectively. The peak frequency of Ferret diameter for all sets of samples is all about 0.07 mm. It indicates most particles are very fine sand. Their frequency distribution appears not changed considerably by seepage.

(3) Frequency Distribution of Major Axis Angle

The major axis angle of a particle is defined as the angle between the major axis of the particle and a prescribed reference direction (taking as the horizontal direction in this paper). The

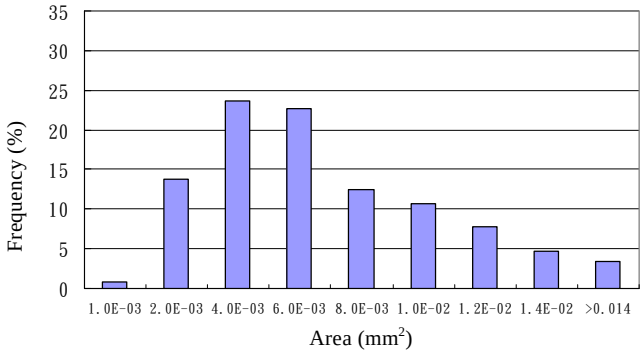

(a) MS1-2

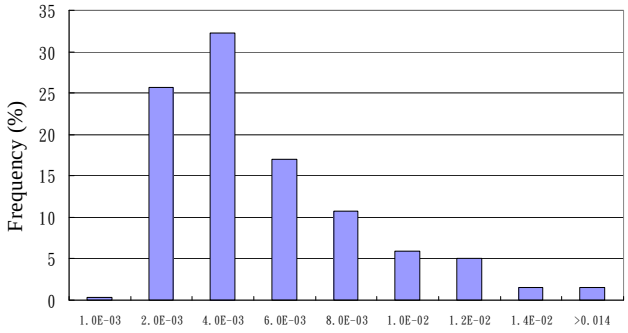

(b) MS3-4

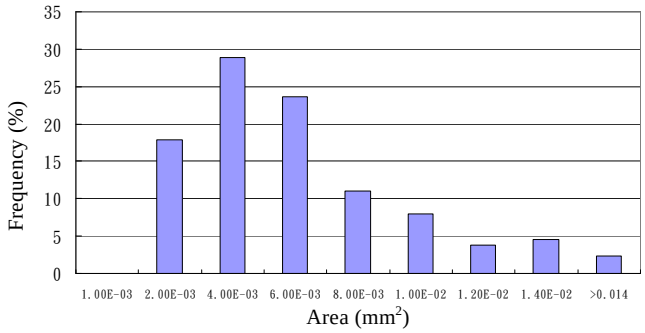

(c) MS5-6

Fig. 18 Distribution of grain area for MS1-2, MS3-4, and MS5-6

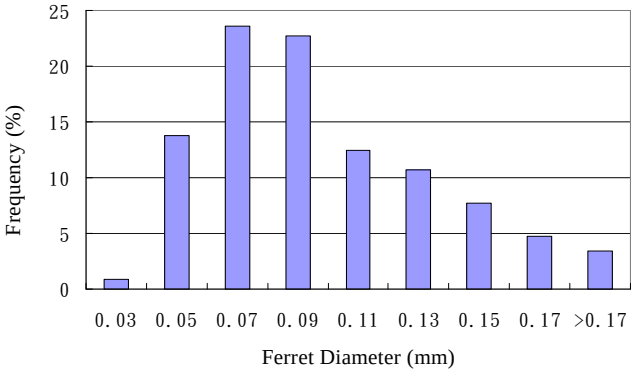

(a) MS1-2

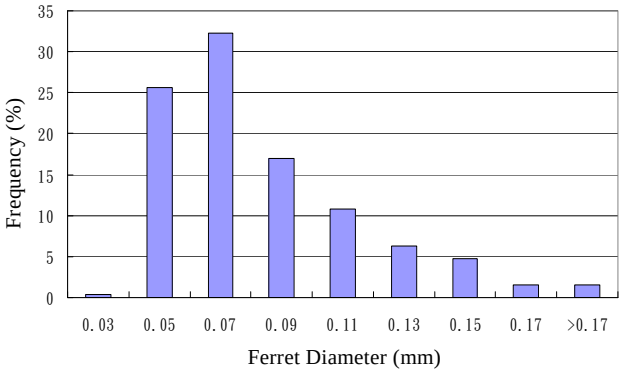

(b) MS3-4

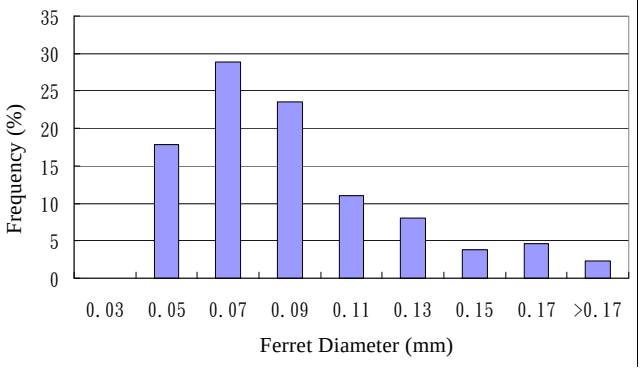

(c) MS5-6

Fig. 19 Distribution of Ferret diameter for MS1-2, MS3-4, and MS5-6

major axis is the axis along which the particle has its largest length. This parameter can be regarded as a measure of particle preferred orientation. Figure 20(a), (b), and (c), respectively, are the distributions of major axis angle obtained from the image sets of MS1-2, MS3-4, and MS5-6, respectively. For all sample sets, it appears the particle orientation remains randomly distributed without obvious preferred orientation.

(4) Frequency Distribution of Particle Elongation

The definition of elongation is the ratio of the major-axis length and the minor-axis length. The major-axis length of a particle is the largest length of the particle along the particle's major axis. The minor-axis length is the largest length of the particle along a direction that is perpendicular to the particle's major axis. A high value of elongation for a particle implies the particle has a slender shape. An elongation near 1.0 means the particle is close to a sphere or a square. Figure 21(a), (b), and (c), respectively, are the distributions of particle elongation obtained from image sets for MS1-2, MS3-4, and MS5-6, respectively. The peak frequency of elongation occurs near 2; and almost all particles have elongation between 1 and 3. It indicates the particle shape in the tested rock material is generally sub-angular or sub-rounded. No change in the distribution of particle orientation before and after seepage is noticeable.

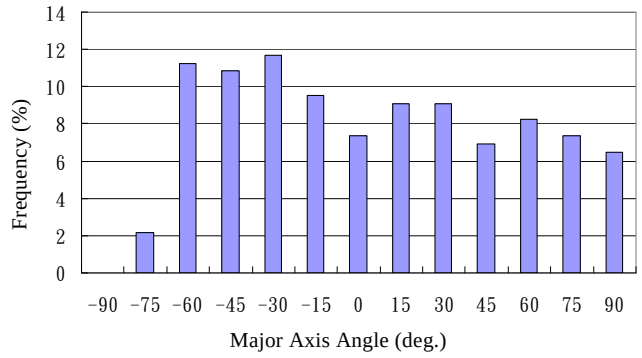

(a) MS1-2

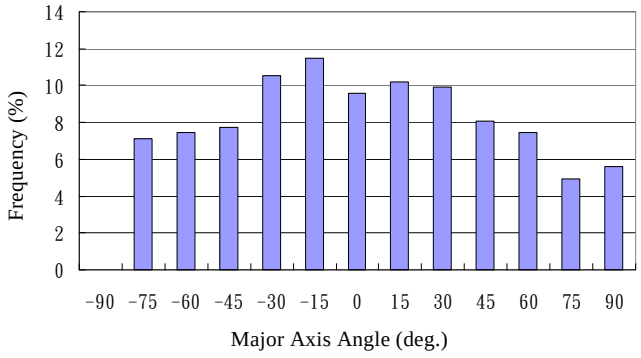

(b) MS3-4

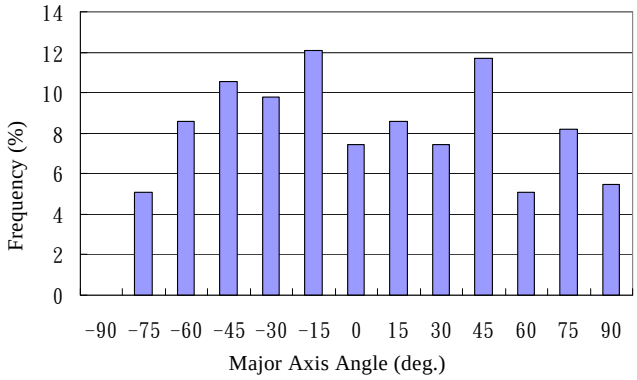

(c) MS5-6

Fig. 20 Distribution of major axis angle for MS1-2, MS3-4, and MS5-6

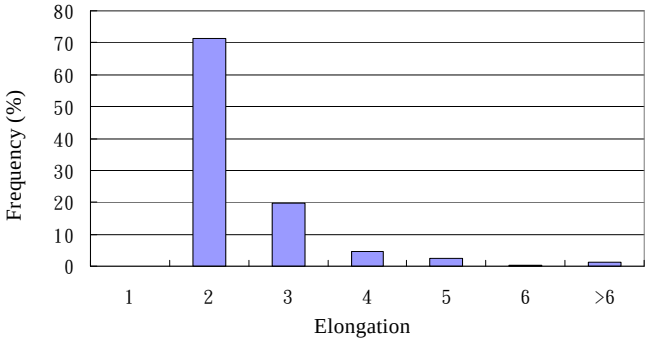

(a) MS1-2

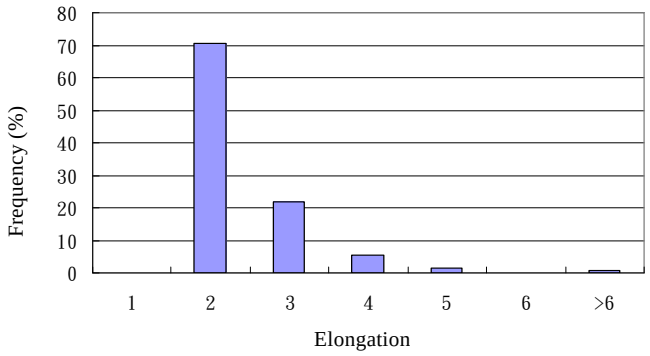

(b) MS3-4

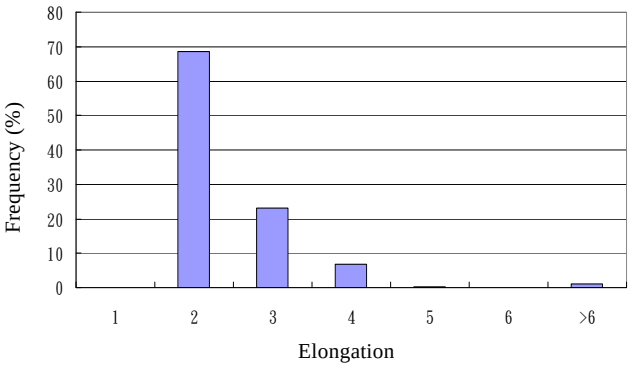

(c) MS5-6

Fig. 21 Distribution of elongation for MS1-2, MS3-4, and MS5-6

(5) Frequency Distribution of Particle Roundness

The particle roundness is defined as $4\pi A/L^2$, in which L denotes the perimeter of the particle. The possible range of roundness is between 0 and 1. It is a measure of the sharpness or angularity of a particle. A higher roundness implies a particle is closer to a sphere; and vice versa. Elongation near 1.0 means the particle is close to a sphere or a square. For a perfect sphere, its roundness is 1.0. Figure 22(a), (b), and (c), respectively, are the distributions of particle roundness obtained from the image sets of MS1-2, MS3-4, and MS5-6, respectively. Most of the particle roundness is within 0.6 ~ 0.8, indicating the particle shape is indeed sub-rounded (instead of sub-angular). The frequency distribution of particle roundness does not show a considerable difference after seepage.

The foregoing text compared the microstructure of the tested samples, including porosity and major texture parameters without and after seepage. It can be observed the porosity significantly increases after the application of seepage possibly due to the wash-away of fines particles or resolved infill material. The increase in porosity is an indication of degradation of rock material. On the other hand, other texture parameters are not affected by the seepage evidently. Their roles on the material degradation due to seepage flow appear less important.

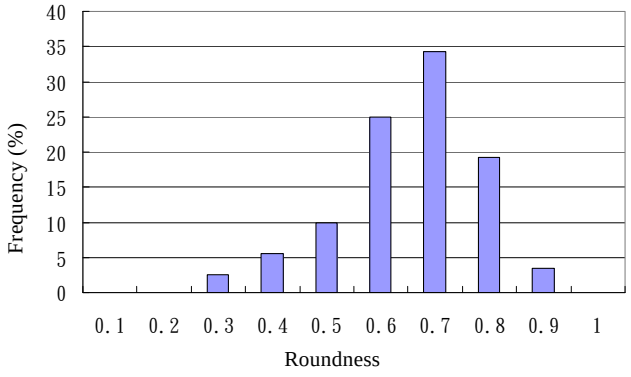

(a) MS1-2

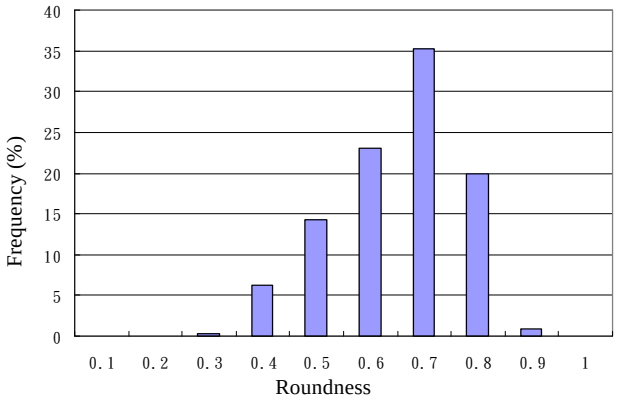

(b) MS3-4

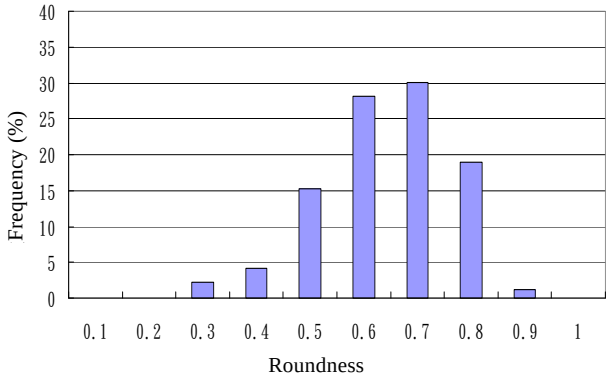

(c) MS5-6

Fig. 22 Distribution of roundness for MS1-2, MS3-4, and MS5-6

5. SUMMARY AND CONCLUSIONS

Fractures or joints are usually much less significant in young soft rock. For soft rock with limited discontinuities, the permeability of intact rock may be close to the in-situ permeability, and the laboratory permeability test can be utilized to determine rock permeability. The permeability determined in the permeability test depends highly on the degree of saturation of the specimen. In the present work, an apparatus was developed for determining rock permeability using the approach of flow pump. The developed apparatus combined the flow-pump and a triaxial cell so that both confining pressure and back-pressure can be applied to the specimen. The added back-pressure enables the control over the degree of saturation of the tested specimen, while the triaxial cell allows the assessment of the effect of confining pressure on permeability. Results from the permeability test verify the capability of the flow-pump apparatus on determining consistent results of the permeability for soft rocks. With the control over the back-pressure, the degree of saturation can be quantitatively controlled. Hence, the results of permeability test will be more reliable. With the control over the confining pressure, the present work also shows the dependency of the permeability of soft rock on confining pressure, loading history, and specimen orientation.

Poorly cemented sandstone usually will degrade when it is exposed to unfavorable environmental conditions. The degradation of weak sandstone may result in the reduction in its strength and deformability. This study also investigates the microstructure change of poorly cemented sandstone due to seepage induced degradation. By comparing the microstructure of sample before and after the seepage, it was found the porosity of sandstone tends to increase after seepage; and the porosity increases with rising hydraulic gradient. Its reason is likely because fines particles or resolved infill materials were moved away as a result of internal erosion due to seepage. On the other hand, other texture parameters (including grain area, Feret diameter, major axis angle, elongation, and roundness) are not affected by seepage with enough evidence.

ACKNOWLEDGEMENTS

The National Science Council of ROC funded the presented work. This financial support is gratefully acknowledged.

REFERENCES

ASTM (1993). “Standard test method for measurement of hydraulic conductivity of saturated porous materials using a flexible wall permeameter.” *Construction: Annual Book of ASTM Standards V4.08*, 151−158.

Huang, A. B., Liao, J. J., Pan, Y. W., and Cheng, M. H. (2001). “Developments in the characterization of soft rocks in Taiwan.” *Proc. 14th Southeast Asia Geotechnical Conference*, Hong Kong.

ISRM (1981). “Rock characterization testing and monitoring.” *ISRM Suggested Methods*, Pergamon Press, New York.

Johnston, I. W. (1993). “Soft rock engineering.” *Comprehensive Rock Engineering: Principles, Practice and Project*, **1**, Pergamon Press, 367−393.

Johnston, I. W. (1995). “Movement of foundations on rock.” *Vertical and Horizontal Deformations of Foundations and Embankment*, ASCE Geotechnical Special Publication, **40**(2), 1703−1717.

Lama, R. D. and Vutukuri, V. S. (1978). *Handbook on Mechanical Properties of Rocks: Testing Techniques and Results*, Trans Tech, Clausthal.

Nikraz, H. R. (1998). “Effect of seepage on the properties of weakly cemented sandstone.” *The Geotechnics of Hard Soils and Soft Rocks*, 273−281.

Nishiyama, T. and Kusuda, H. (1994). “Identification of pore spaces and microcracks using fluorescent resins.” *Int. J. Rock Mech. Min. Sci. and Geomech. Abstr.*, **31**(4), 369−375.

Ocepek, D. and Logar, J. (2008). "Failure mechanism following peak strength in carboniferous-permian soft rock." *Proc. 42nd US Rock Mechanics Symposium*, San Francisco.

Oliveira, R. (1993). "Weak rock materials." *The Engineering Geology of Weak Rock*, 5–15.

Olsen, H. W., Morin, R. H. and Nichols, R. W. (1988). "Flow pump application in triaxial testing." *Advanced Triaxial Testing of Soil and Rock*, ASTM STP 977, 68–81.

Tatsuoka, F. and Kohata, Y. (1995). "Stiffness of hard soils and soft rock in engineering application." *Proc. 1st International Symposium on Pre-failure Deformation of Geo-materials*, Sapporo, Japan, 947–1066.

Tatsuoka, F., Hayano, K. and Koseki, J. (2003). "Strength and deformation characteristics of sedimentary soft rock in the Tokyo metropolitan area." *Proc. Characterization and Engineering Properties of Natural Soils*, Swets and Zeitlinger, Lisse.

Wilbur, B. C. (1990). *The Influence of Normal Stress on Fracture Transmissivity*, Master Thesis, Colorado School of Mines.